Impact of microstructure on the effective diffusivity in random packings of hard spheres

Cite as: J. Appl. Phys. **116**, 034904 (2014); https://doi.org/10.1063/1.4889821
Submitted: 12 June 2014 . Accepted: 28 June 2014 . Published Online: 16 July 2014

H. Liasneuski, D. Hlushkou, S. Khirevich, A. Höltzel, U. Tallarek, and S. Torquato

Impact of microstructure on the effective diffusivity in random packings of hard spheres

H. Liasneuski,[1,2,a)] D. Hlushkou,[1,3,a)] S. Khirevich,[1] A. Höltzel,[1] U. Tallarek,[1,b)] and S. Torquato[4,b)]

[1]*Department of Chemistry, Philipps-Universität Marburg, Hans-Meerwein-Strasse, 35032 Marburg, Germany*
[2]*Department of System Analysis and Computer Simulation, Belarusian State University, Kurchatov Street 5, 220050 Minsk, Belarus*
[3]*Max-Planck-Institut für Dynamik komplexer technischer Systeme, Sandtorstr. 1, 39106 Magdeburg, Germany*
[4]*Department of Chemistry, Department of Physics, Program in Applied and Computational Mathematics, Princeton Institute for the Science and Technology of Materials, Princeton University, Princeton, New Jersey 08544, USA*

(Received 12 June 2014; accepted 28 June 2014; published online 16 July 2014)

We present results of computer simulations of the effective diffusion coefficient in bulk random packings of hard monosized spheres with solid volume fraction between 0.54 (random-loose packing) and 0.634 (maximally random jammed). Six types of sphere packings were generated with different protocols and parameters resulting in a systematically varied degree of microstructural heterogeneity. The packing morphology is qualitatively characterized by statistical analyses of Voronoi cells obtained from spatial tessellation of the packing space. Diffusive transport of point-like tracers in the pore space of the packings was simulated with a random-walking particle-tracking technique. Our results indicate that the effective transport characteristics of the random sphere packings are not fully defined from the solid volume fraction but also depend on the packing microstructure. For the first time, we compared (i) the values of the effective diffusion coefficient D_{eff} simulated in packings with different morphologies, and (ii) the corresponding values of D_{eff} obtained from an approximate analytical formula involving the three-point microstructural parameter ζ_2. This analysis reveals that this approximation involving ζ_2 clearly reflects key morphological specificity of individual sphere packings and provides a sufficiently accurate estimate of the effective diffusion coefficient.
[http://dx.doi.org/10.1063/1.4889821]

I. INTRODUCTION

The determination of the effective physical properties of an inhomogeneous medium composed of different materials or phases is a problem of great interest in industrial, biological, and environmental processes like catalysis, filtration, oil recovery, ground water remediation, chromatography, transport through cell membranes, solar energy production, fabrication of composite materials, etc.[1–4] Generally, the determination of effective properties of a multi-phase medium requires knowledge of the phase interface geometry and physical properties of the individual phases. Many physical transport properties in a macroscopically (i.e., statistically) isotropic medium can be described by a linear relationship between the average of a generalized local "flux" $\mathbf{J}$ and the average of a generalized local "intensity" $\mathbf{G}$[1]

$$\mathbf{J} \propto K_{\text{eff}}\mathbf{G}, \tag{1}$$

where K_{eff} is an effective property (or effective transport coefficient) of the medium. For instance, for the electrical conduction and diffusion problems, $\mathbf{J}$ represents the average electric current density and average diffusive flux, respectively, and $\mathbf{G}$ represents the average local electric field and average negative gradient of the local concentration, respectively. For these two problems, the coefficient in Eq. (1) is the effective electrical conductivity and the effective diffusion coefficient, respectively. Linear relationships similar to Eq. (1) can be established as well for thermal conduction and magnetostatic problems. In spite of the functional simplicity of Eq. (1), its direct application to transport phenomena in microscopically inhomogeneous media is hampered. In a heterogeneous material consisting of several phases, K_{eff} depends not only on properties and volume fractions of the individual phases but also on the microstructural details. Complete information on the morphology of a heterogeneous medium is commonly very difficult or impossible to be accessed experimentally. Alternatively, the microstructure can be also completely characterized by an infinite set of correlation functions or n-point probability functions.[3,5] These functions were introduced by Brown in the context of determining the effective properties of random heterogeneous media.[6] However, such a complete statistical information is never known even for the simplest class of disordered composite media, such as random arrays of parallel hard cylinders.

A useful alternative to predict effective properties of heterogeneous media is the determination of rigorous lower and upper bounds on effective coefficients, which require only limited microstructural information. Bounds which

[a)]H. Liasneuski and D. Hlushkou contributed equally to this work.
[b)]Authors to whom correspondence should be addressed. Electronic addresses: tallarek@staff.uni-marburg.de and torquato@electron.princeton.edu.

incorporate microstructural information up to the n-point level commonly are referred to as "n-point" or "nth-order" bounds. As successively more microstructural information is included, the bounds become progressively narrower.[1,5] Several methods and techniques have been developed to derive bounds on effective transport coefficients, e.g., variational principles,[7–11] the method of Padé approximants,[12–14] the translation method,[15–19] and the field equation recursion method.[20] Specifically for macroscopically isotropic composites, Hashin and Shtrikman derived the best possible two-point bounds on the effective magnetic permeability, given just volume-fraction information.[21] For reasons of mathematical analogy, the same bounds can be applied to electrical or heat conductivity and diffusivity. Later, Beran derived bounds for two-phase isotropic composites, which involve sixfold integrals of certain three-point correlation functions and improve the Hashin-Shtrikman bounds.[9] Torquato[22] and Milton[23] independently showed that the three-point Beran bounds can be expressed in terms of the volume fractions and the single three-point microstructural parameter ζ_2, which is a multidimensional integral involving the three-point probability function. The Beran bounds were derived using trial fields based on the first two terms of the exact perturbation expansion. For the special case of a dispersion of identical penetrable (i.e., overlapping) spherical particles, Torquato derived three-point bounds, utilizing trial fields based on the first two terms of the exact cluster expansion.[24] It has been shown[25] that the Beran and Torquato bounds are identical for dispersions of monosized hard (impenetrable) spheres and they both depend on the microstructural parameter ζ_2. The same parameter is involved in an approximate formula for the effective conductivity of dispersions of inclusions with a polydispersity in size.[14] The formula was shown to be highly accurate provided that the inclusions, generally, do not form large clusters. This approximation is referred to as a three-point approximation as it incorporates information up to three-point correlation functions.

Though n-point bounds becomes tighter as n increases and further morphological information is accounted for, the calculation of even three-point bounds is a challenging task for real heterogeneous materials. An alternative to theoretical approaches of evaluating effective properties of heterogeneous media is their numerical simulation. The evaluation of effective properties via computer simulations is commonly a two-step process. First, one acquires a complete description of the medium microstructure. It can be obtained either via computer-generation of a material or by physical reconstruction of the real structure. Several imaging techniques are nowadays available to investigate the three-dimensional structure of porous media.[26] Their capabilities range, e.g., from nanometer resolution with techniques based on electron microscopy,[27–31] through micron and submicron scale with X-ray tomography[32–35] and confocal laser scanning microscopy,[36–40] to several tens of micrometers with nuclear magnetic resonance imaging.[41–44] Second, the effective properties of a material are determined either by the numerical solution for the local governing equations describing a transport phenomenon, or by direct numerical simulation of the transport process.

In this contribution, we present results of direct numerical simulations of diffusive transport in bulk, monodispersed, random hard-sphere packings over a range of the solid volume fraction $\phi = 0.54$–0.634, i.e., from random-loose to random-close packing, the latter of which more recently is sometimes referred to as the maximally random jammed packing.[45] By a variation of the packing generation algorithm and its parameters, we generated six distinct packing types that differ in the individual arrangement of the spheres even at identical ϕ. Diffusion in the void space of the packings was simulated by a random-walk particle-tracking (RWPT) technique. Then, the effective diffusion coefficient D_{eff} was determined for each packing type and solid volume fraction. This approach allowed us to evaluate how the resulting D_{eff}–ϕ curves reflect the different packing microstructures. For the first time, the values of D_{eff} obtained by simulation of diffusive transport in the void space of random sphere packings characterized by different microstructures are compared with D_{eff} calculated from a three-point approximation due to Torquato involving the microstructural parameter ζ_2.[13]

The paper is organized as follows. In Sec. II, we describe briefly one-, two-, and three-point bounds on the effective diffusion coefficient in a macroscopically isotropic two-phase medium. A three-point approximation of D_{eff} in monosized sphere packings, based on the microstructural parameter ζ_2, is also given. In Sec. III, we provide the simulation details for (i) generation of random sphere packings with different microstructures, (ii) determination of the effective diffusion coefficient, and (iii) calculation of the three-point microstructural parameter ζ_2. In Sec. IV, we report simulation results for D_{eff} in the random packings and compare the obtained values with the three-point approximation. Effective diffusion coefficients simulated in two regular (simple cubic and face-centered cubic) arrays of spheres are analyzed to validate the employed numerical approaches, using analytical results for D_{eff} and ζ_2. Finally, conclusions and comments are presented in Sec. V.

II. BOUNDS AND APPROXIMATION FOR THE EFFECTIVE DIFFUSIVITY

Here, we give a brief review of the bounds on the effective diffusion coefficients in packings of hard spheres. For reasons of mathematical analogy of effective media problems, these bounds can be directly obtained from the already known bounds derived for the effective conductivity (as well as for the magnetic permeability or dielectric constant) of two-phase materials. The effective conductivity or effective diffusion coefficient is characterized by transport properties of the whole medium, i.e., contributions from both phases to the overall transport process are explicitly accounted for. However, if one phase, say phase 2, is impermeable (transport vanishes) and diffusion only occurs in phase 1, then the effective conductivity or diffusion coefficient must be divided by a factor of $(1-\phi)$,[46] where ϕ is the volume fraction of phase 2, which we take to be the space occupied by spheres.

Let us consider a packing of hard spheres as a material composed of two phases, phase 1 (space outside of the

spheres) and phase 2 (spheres). Each constituting phase is characterized with the corresponding volume fraction, $(1-\phi)$ and ϕ, respectively, and the diffusion coefficients D_1 and D_2. In a two-phase composite material, the one-point lower and upper bounds ($D_L^{(1)}$ and $D_U^{(1)}$, respectively) on the effective diffusion coefficient are[1,21,47]

$$D_L^{(1)} = \frac{D_1 D_2}{[(1-\phi)D_2 + \phi D_1](1-\phi)} \quad \text{and}$$
$$D_U^{(1)} = \frac{D_1(1-\phi) + D_2\phi}{1-\phi}. \tag{2}$$

Adapting Eqs. (2) to packings of *impermeable* hard spheres (i.e., assuming $D_2 = 0$), we obtain

$$0 \le D_{\text{eff}} \le D_1. \tag{3}$$

Obviously, the one-point bounds Eqs. (2) and (3) provide no useful information for the estimation of D_{eff} in this case.

Hashin and Shtrikman derived improved bounds for an isotropic two-phase medium,[21] which are the best possible bounds given just ϕ. Although only volume-fraction information is explicitly involved in the expressions for these bounds, it has been shown that they incorporate implicitly the two-point probability function in a trivial manner: For isotropic media, the integral which is used to calculate the bounds, involving the two-point probability function, just depends on the integration interval, i.e., ϕ and ϕ^2.[1] Thus, these bounds are actually contain two-point information. The Hashin–Shtrikman lower and upper bounds ($D_L^{(2)}$ and $D_U^{(2)}$, respectively) for the effective diffusion coefficient are given by

$$D_L^{(2)} = \frac{D_2}{1-\phi}\frac{1+2(1-\phi)\beta_{12}}{1-(1-\phi)\beta_{12}} \quad \text{and}$$
$$D_U^{(2)} = \frac{D_1}{1-\phi}\frac{1+2\phi\beta_{21}}{1-\phi\beta_{21}} \tag{4}$$

with

$$\beta_{ij} = \frac{D_i - D_j}{D_i + 2D_j}. \tag{5}$$

For packings impermeable hard spheres, Eqs. (4) and (5) are reduced to the following two-point bounds:

$$0 \le D_{\text{eff}} \le \frac{D_1}{1+0.5\phi}. \tag{6}$$

Although the upper two-point bound in Eq. (6) depends on the sphere volume fraction, it was shown that this bound is substantially restrictive only in a relatively small range of ϕ.[48,49] Further improvement of the bounds can be achieved if a more detailed description of packing morphology is involved. Three-point bounds account for phase arrangement in a heterogeneous medium. Beran[9] developed three-point bounds on the electric conductivity of an isotropic two-phase composite, subsequently simplified independently by Torquato[22] and Milton,[23] which can be adapted for the effective diffusion coefficient as follows:

$$0 \le D_{\text{eff}} \le D_1\left(1 - \frac{\phi}{\phi + 2(1-\zeta_2)}\right), \tag{7}$$

where ζ_2 is the three-point microstructural parameter defined by the expression

$$\zeta_2 = 1 - \frac{1}{16\phi(1-\phi)\pi^2}\int\int d\mathbf{r}_{12}d\mathbf{r}_{13}\frac{P_2(\cos\theta)}{r_{12}^3 r_{13}^3} \times \left[S_3(r_{12}, r_{13}, r_{23}) - \frac{S_2(r_{12})S_2(r_{13})}{S_1}\right]. \tag{8}$$

The quantities $S_2(r_{12})$ and $S_3(r_{12}, r_{13}, r_{23})$ are, respectively, the probabilities of finding in the interparticle void space the end points of a line segment of length r_{12} and the vertices of a triangle with sides of length r_{12}, r_{13}, and r_{23}; θ is the angle opposite to the side of length r_{23} and P_2 is the Legendre polynomial of order two.

We want to point out that the one-, two-, and three-point lower bounds in Eqs. (3), (6), and (7) are equal to zero because they correspond to microstructures in which the nondiffusive phase 2 ($D_2 = 0$) is topologically connected while the diffusive phase 1 ($D_1 \neq 0$) is disconnected.[1] In packings of hard spheres, the ratio between the diffusion coefficients within and outside the spheres is equal to zero. As a consequence, only the upper bounds remain finite and may provide a reasonable estimate of the effective diffusion coefficient in hard-sphere packings.

Torquato developed an accurate approximation formula for the effective conductivity of a broad class of particle dispersions,[13] including sphere packings, that involves the three-point parameter ζ_2. In the special limit corrresponding to an impermeable particle phase ($D_2 = 0$), this formula leads to the following analytical approximation for the effective diffusion coefficient:[13]

$$D_{\text{eff}} \approx \frac{D_1}{1-\phi}\frac{1+2\phi\beta_{21} - 2(1-\phi)\zeta_2\beta_{21}^2}{1-\phi\beta_{21} - 2(1-\phi)\zeta_2\beta_{21}^2}. \tag{9}$$

It was shown[13] that the value of D_{eff} calculated with Eq. (9) does not exceed the three-point upper bound (cf. Eq. (7)).

III. NUMERICAL SIMULATIONS

A. Packing generation and microstructure characterization

Isotropic random packings of monosized, hard, impermeable spheres were generated in rectangular simulation boxes with dimensions of $\sim 10 \times 10 \times 70$ sphere diameters (d_p) and with periodic boundary conditions which ensure continuity at all box boundaries. The number of spheres in the packings varied from 7219 up to 8476 depending on the targeted solid volume fraction ϕ. For packing generation, two approaches based on the Jodrey–Tory[50] and Monte Carlo (MC)[51–53] algorithms were employed.

The Jodrey–Tory (JT) algorithm is a collective-rearrangement generation method,[54] which yields geometrically jammed, but mechanically unstable packings. The relevant feature of the JT-algorithm is that it yields macroscopically isotropic packings where partial

crystallization is avoided.[55] For this study, we used a modified JT-algorithm[52] allowing to vary systematically the degree of heterogeneity (DOH) of the packing microstructure through the generation parameters. Packing generation with the modified JT-algorithm starts from a random distribution of points representing sphere centers in a simulation box, where sphere overlap is typical. Then, the iterative packing procedure starts. Each iteration consists of two steps: (i) the search for two sphere centers c_i and c_j with minimum pair-wise distance $d_{ij,\min}$ that defines the maximal sphere diameter at which no sphere-overlap occurs in the current configuration, and (ii) symmetrical spreading apart of these two sphere centers along a line c_ic_j up to the new distance $d_{ij,\max} = d_{ij,\min} + \Delta_{ij}$ determined as

$$d_{ij,\max} = d_{ij,\min} + \Delta_{ij} = d_{ij,\min}\left(1 + \alpha \log_{10}\frac{d_p}{d_{ij,\min}}\right), \quad (10)$$

where α is a scaling constant for the spreading length. As $d_{ij,\min}$ asymptotically approaches d_p, the current solid volume fraction approaches the targeted (final) value of ϕ. Four different JT-packing types were generated by varying (i) the initial distribution scheme of the sphere centers and (ii) the value of the scaling constant α. Generation of R-packings started from a random and uniform distribution of sphere centers in the simulation box, whereas for S-packings the simulation box was first divided into N equal cubes (where N is the number of spheres) and then each sphere center was placed in a random position into a cube. The scaling constant was set to $\alpha = 0.001$ (these packings are referred to as $R \times 0.001$ packings), $\alpha = 1$ ($R \times 1$ and $S \times 1$ packings), or $\alpha = 2$ ($S \times 2$ packings). With a small spreading length, the sphere centers remain close to their initial positions during packing generation, preserving the randomness of the initial distribution. A larger spreading length yields a more homogeneous distribution of sphere centers in the final configuration.

To illustrate the effect of the varied JT-packing generation parameters on the final packing microstructure, we use a two-dimensional representation, i.e., random packings of uniform disks instead of spheres. Figure 1 visualizes the two-step parameter variation used for packing generation with the Jodrey–Tory algorithm to yield the four JT-packing types $R \times 0.001$, $R \times 1$, $S \times 1$, and $S \times 2$. (The $S \times 2$ packing is replaced by an $S \times 6$ packing in Fig. 1 to achieve a stronger visual effect.) S-packing generation starts from a more ordered (lattice-based) initial distribution of sphere centers than R-packing generation, and the value of the constant for scaling the displacement length $\alpha = 6$ ($\alpha = 2$ for sphere packings), $\alpha = 1$, or $\alpha = 0.001$ determines how well inhomogeneities in the initial distribution of sphere centers are balanced out in the final packing microstructure. It is important to recognize from Fig. 1 that the parameter variation used with the JT-algorithm operates on two different length scales: the initial ordered or random distribution of the sphere centers concerns the whole packing, whereas the value of the scaling constant α affects the local environment of the individual spheres in a packing.

The MC method[51–53] provides a complementary approach to the JT-algorithm for generating dense, random sphere packings. This method is similar to that developed by Metropolis *et al*. to investigate equations of state for systems with hard interacting particles.[56,57] MC-packing generation starts from a uniform distribution of spheres arranged in a dilute cubic array constructed from expanding a simple cubic lattice.[51,52] We used an expansion factor of 2, resulting in an eight times larger volume of the initial packing compared with a simple cubic packing. The packing spheres are moved in random directions and each move that does not result in a collision with another sphere is accepted. The desired solid volume fraction ϕ is reached by compression of the coordinate system, executed every 5000 movement attempts. For this purpose, the minimal distance between sphere centers $d_{\min}$ is determined and the simulation box is scaled by the factor $d_p/[d_p + \Omega(d_{\min} - d_p)]$ while keeping the sphere diameters constant. Here, Ω is the compression rate. By using $\Omega = 0.95$ (fast compression) or $\Omega = 0.05$ (slow compression), we generated two different MC-packing types, $\Omega \times 0.95$ and $\Omega \times 0.05$, respectively. The values of Ω were chosen from the ends of the possible range ($0 < \Omega \leq 1$) to create a maximum of microstructural variety with the two MC-packing types. The MC-algorithm is known to incorporate crystalline regions into a packing, if low compression rates and large solid volume fractions are combined.[55,58]

By variation of the packing generation algorithms and their parameters, we generated six distinct types ($S \times 2$, $S \times 1$, $R \times 1$, $R \times 0.001$, $\Omega \times 0.05$, and $\Omega \times 0.95$) of monodisperse, bulk, random sphere packings. Each packing type was generated at six solid volume fractions ($\phi = 0.54$, 0.56, 0.58, 0.60, 0.62, 0.634) with one exception: we were not able to generate $S \times 2$ packings at $\phi = 0.634$. To account for statistical variations, ten realizations of each packing type and solid volume fraction were generated, 350 packings in total. Results reported for a packing of a given type and solid volume fraction refer to the mean value from the ten individual realizations. The number of realizations together with the extended packing dimensions ensured a thorough sampling of the structural variations among individual packings of the same type and porosity.

To evaluate the DOH of the generated packings, we employ Voronoi tessellation, which is widely accepted as a powerful tool to analyze the microstructure of disordered systems.[59–65] Voronoi tessellation surrounds each sphere in a monodisperse packing by a polyhedron that contains all points closer to this sphere center than to any other. The packing space is thus divided into a set of non-overlapping polyhedra with associated Voronoi volumes V_V. It was shown that the packing structure can be characterized by the properties of Voronoi polyhedra. Oger *et al*. investigated the topological and metric properties of Voronoi polyhedra in random sphere packings as a function of ϕ.[66] They showed that the V_V-distribution becomes narrower and more symmetric at higher packing density. Gil Montoro and Abascal[67] employed Voronoi tessellation to study the microstructure of several simple fluids, such as the Lennard–Jones fluid at two thermodynamic points corresponding to solid and liquid phases, two differently quenched supercooled states obtained from the liquid, and ideal gas. The authors revealed that the skewness of the V_V-distributions properly reflects the

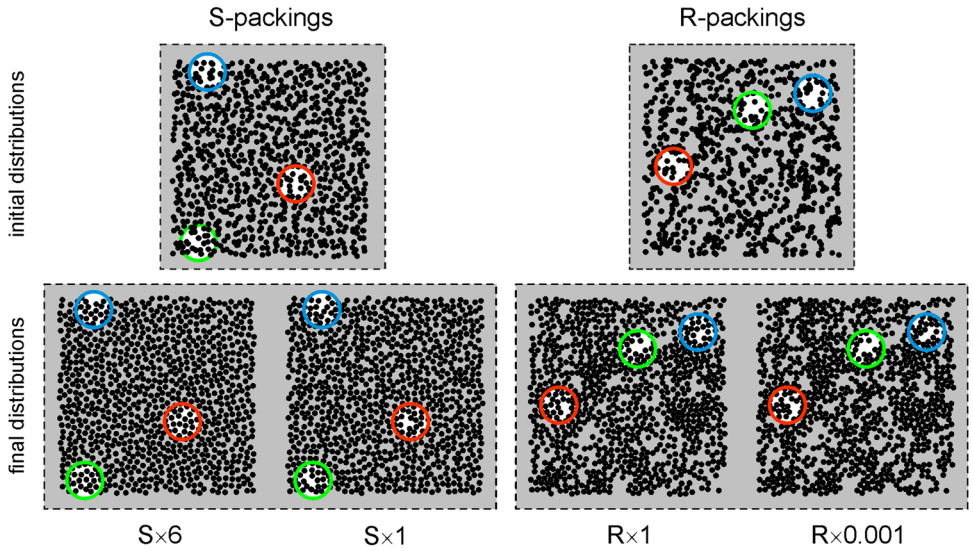

FIG. 1. Bulk random packings of monosized hard disks at $\phi \approx 0.54$ generated with the Jodrey–Tory algorithm following different packing protocols. Shown are the initial distributions of the disks for S- and R-packings (top) and final distributions for S × 6, S × 1, R × 1, and R × 0.001 packings (bottom). Colored circles aid the comparison between the initial and final packing microstructures.

heterogeneity of the particle neighborhood and clearly discriminates between systems: The more homogeneous a system the smaller is the skewness of the V_V-distribution.

Figures 2(a) and 2(b) show standard deviation σ and skewness γ, respectively, of the V_V-distributions for the generated packings. The two parameters $\sigma(V_V)$ and $\gamma(V_V)$ are quantitative measures for the microstructural DOH of a packing. Each of the six packing types has a unique ϕ-scaling of the DOH. For the four JT-packing types, it reflects their relative packing-scale disorder: $R \times 0.001 > R \times 1 > S \times 1 > S \times 2$, i.e., the higher the packing-scale disorder, the higher the values of $\sigma(V_V)$ and $\gamma(V_V)$ at a given solid volume fraction and the steeper the rise of these two parameters at decreasing ϕ. MC-packings are more homogeneous than the most homogeneous JT-packing type ($S \times 2$) at low to intermediate solid volume fractions ($\phi = 0.54$–0.6) and for the $\Omega \times 0.95$ packing type this remains the case also at high solid volume fractions ($\phi = 0.62$–0.634). Given that MC-packing generation starts from a lattice-based distribution of sphere centers, this result is not unexpected. Whereas the $\Omega \times 0.95$ packing type follows essentially the same trend upon densification as the JT-packing types, i.e., the DOH decreases, only with a smaller slope, the $\Omega \times 0.05$ packing type behaves quite differently: Its DOH goes through a minimum at $\phi = 0.60$ and then increases again, so that at $\phi = 0.634$ the $\Omega \times 0.05$ packing has the highest DOH among all packing types. This high DOH is explained by the irregular distribution of dense and more loosely packed regions, which translates to increased disorder on the packing scale.

B. Simulation of diffusion

Diffusion in the generated packings was simulated by a RWPT technique,[68] employing a multiple-rejection boundary condition at the solid-liquid interface.[69] Initially, an ensemble of 5×10^6 point-like tracer particles was randomly distributed within the void space of a packing, and then displaced due to random motion calculated from a Gaussian

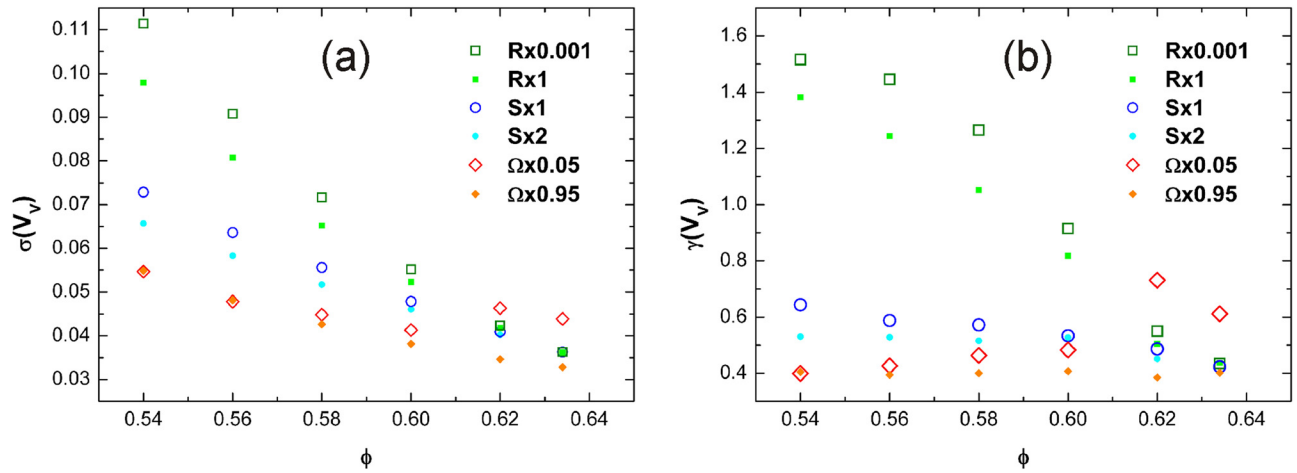

FIG. 2. Standard deviation (a) and skewness (b) of the Voronoi volume distributions for the generated sphere packings as a function of the solid volume fraction.

distribution with a mean of zero and a standard deviation of $(2D_1\delta t)^{1/2}$ around each spatial coordinate. The position of all tracers was monitored at each time step δt, defined such that the maximum tracer displacement at each iteration did not exceed a distance of $d_p/60$. Diffusion coefficients $D(t)$ in a given direction were calculated from the tracer displacements[70] as

$$D_x(t) = \frac{1}{2N}\frac{d}{dt}\sum_{i=1}^{N}(\Delta r_{xi} - \langle \Delta r_x \rangle)^2, \tag{11}$$

where Δr_{xi} and $\langle \Delta r_x \rangle$ denote the corresponding Cartesian components of the displacement of the ith tracer and the average displacement of the tracer ensemble after time t, respectively, in x-direction. Isotropic diffusion behavior was observed for all packing types. The effective diffusion coefficients D_{eff} were determined from asymptotes of the $D(t)/D_1$-curves, shown for selected packings in Fig. 3.

The program realization of the RWPT-algorithm was implemented as a parallel code in C language using the Message Passing Interface (MPI) standard.[71] The total simulation time for all packings was ~24 h on 512 BlueGene/P processor cores.

C. Determination of ζ_2

The determination of the three-point correlation function S_3 needed to calculate ζ_2 is a nontrivial computational task. In this study, we used a numerical approach proposed by Miller and Torquato to determine ζ_2 for packings of identical hard spheres.[72] The authors showed that this three-point microstructural parameter can be calculated as

$$\zeta_2 = \frac{\langle \mathbf{E}\cdot\mathbf{E}I\rangle}{2\phi(1-\phi)\beta_{21}^2\langle \mathbf{E}\rangle\cdot\langle \mathbf{E}\rangle} - \frac{1-\phi}{2}. \tag{12}$$

In Eq. (12), $I(\mathbf{r})$ is the indicator function, defined to be

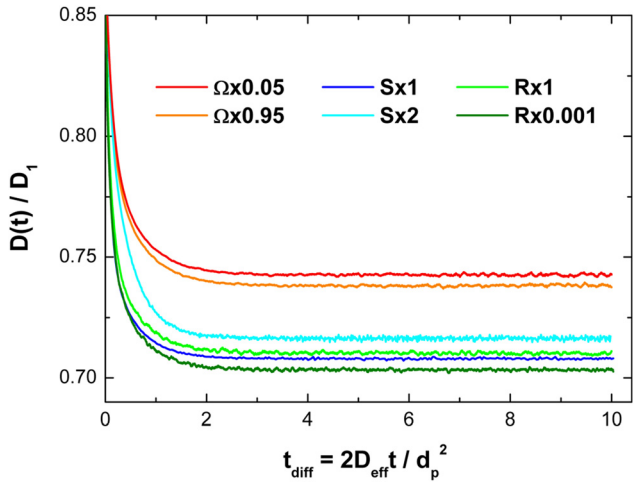

FIG. 3. Time-evolution of the normalized diffusion coefficient $D(t)/D1$ for selected packings at $\phi = 0.56$. Elapsed time is given in units of the diffusive time defined as $t_{diff} = 2D_{eff}/d_p^2$, where D_{eff} is the asymptotic (long-time) value of the diffusion coefficient in a sphere packing and d_p is the sphere diameter. One diffusive time unit is the time it takes for a tracer to travel an average distance equal to one sphere diameter.

$$I(\mathbf{r}) = \begin{cases} 1, & \text{if } \mathbf{r} \in \text{ interior of the spheres} \\ 0, & \text{otherwise} \end{cases} \tag{13}$$

and $\mathbf{E}(\mathbf{r})$ is the trial fluctuation field defined for a system of N spheres centered at positions $\mathbf{r}^N \equiv \mathbf{r}_1,\mathbf{r}_2,\ldots,\mathbf{r}_N$ as

$$\mathbf{E}(\mathbf{r};\mathbf{r}^N) = \sum_{i=1}^{N}\mathrm{K}(\mathbf{x}_i)\cdot\langle \mathbf{E}\rangle - \int d\mathbf{r}_1\rho\mathrm{K}(\mathbf{x}_1)\cdot\langle \mathbf{E}\rangle, \tag{14}$$

where ρ is the number density of the spheres and K is the single-body operator

$$\mathrm{K}(\mathbf{r}) = \begin{cases} \beta_{21}d_p^3/8r^3(3\hat{\mathbf{r}}\hat{\mathbf{r}} - \mathrm{A}), & r > d_p/2 \\ -\beta_{21}\mathrm{A}, & r < d_p/2 \end{cases}. \tag{15}$$

Here, $\mathbf{x}_i = \mathbf{r} - \mathbf{r}_i$, $\mathrm{r} = |\mathbf{r}|$, $\hat{\mathbf{r}} = \mathbf{r}/\mathrm{r}$, and A is the unit dyadic. The angular brackets in Eqs. (12) and (14) denote an average over the sphere ensemble. Equations (12)–(15) provide a mean to determine ζ_2, which does not require direct sampling of the three-point probability function S_3.

Sampling for ζ_2 was carried out with 5 different sets of 200 000 points randomly distributed in each individual packing. The periodic boundary condition was employed to approximate an infinite system. First, the value of K is calculated for each random point and each of the N spheres in a packing according to Eq. (15). After all spheres have been sampled, the quantities $\mathbf{E}$ and $\mathbf{E}\cdot\mathbf{E}I$ are calculated and the next sample point is chosen. ζ_2 is then determined by use of Eq. (12). The values of ζ_2 for a given sphere packing and 5 different point sets differ by less than 0.1%.

IV. RESULTS AND DISCUSSION

A. Regular packings

To validate the numerical approaches we used to simulate the effective diffusion coefficients and determine ζ_2, we started from the analysis of D_{eff} in regular arrays of spheres. The values of D_{eff} and ζ_2 for periodic arrangement of hard spheres can be determined analytically. Specifically, McPhedran and Milton computed ζ_2 for three cubic lattices of spheres as a function of ϕ.[73] In Figs. 4(a)–4(b), we compare values of ζ_2 for SC and FCC sphere arrays calculated by the numerical approach described in Sec. III C (open circles) and the values obtained analytically by McPhedran and Milton (solid circles).[73] The data in Fig. 4 indicate that the numerical approach by Miller and Torquato[72] allows one to determine ζ_2 with high accuracy over a wide range of the solid volume fraction, including the close packing limit, $\phi \approx 0.524$ and 0.741 for SC and FCC, respectively.

Further, we employed the calculated values of ζ_2 to estimate effective diffusion coefficients in the SC and FCC sphere arrays according to Eq. (9). Alternatively, effective diffusion coefficients in SC and FCC sphere packings can be determined with an analytical approach developed by Blees and Leyte.[74] In Figs. 5(a) and 5(b), we compare D_{eff} in SC and FCC sphere arrays (i) obtained by the analytical approach, (ii) determined with Eq. (9), and (iii) simulated by the RWPT method described in Sec. III B. For both types of

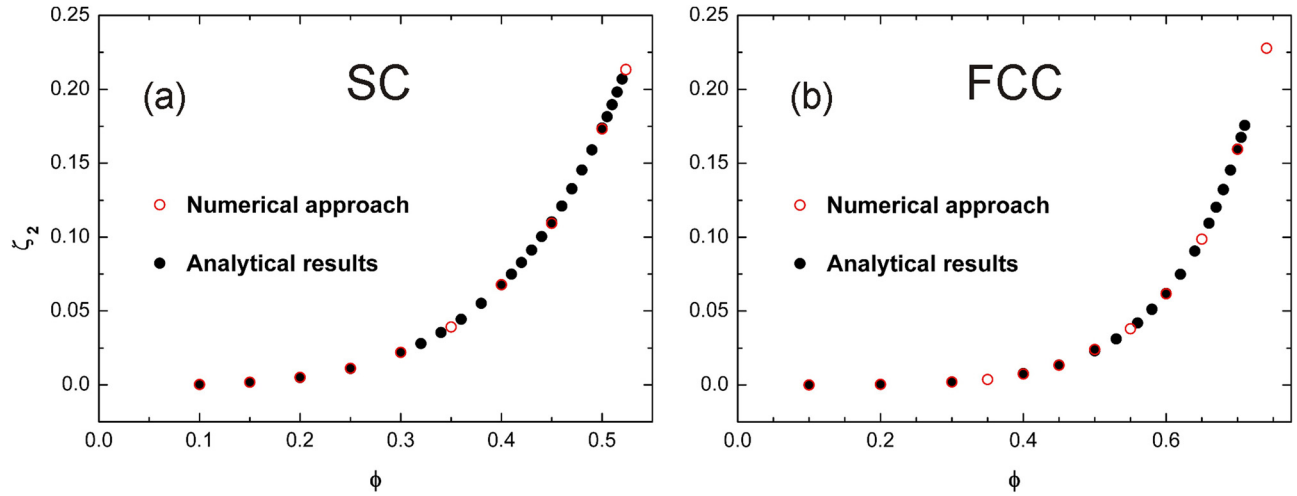

FIG. 4. Comparison of the values for the three-point microstructural parameter ζ_2 obtained by the numerical approach (Ref. 72; open circles) and calculated with the analytical approach (Ref. 73; solid circles) for SC and FCC sphere arrays as a function of the solid volume fraction.

regular packings, the results obtained by the RWPT simulations are in excellent agreement with those calculated using the analytical approach by Blees and Leyte[74] over the whole range of ϕ. This enables us to conclude that our simulation approach can determine accurately effective diffusion coefficients of these ordered spheres packings. At low values of ϕ, Eq. (9) also provides a quite precise approximation of D_{eff}. The accuracy decreases slightly with increasing packing density such that it slightly overestimates such values of D_{eff}.

B. Random packings

We employed the RWPT simulations to determine the effective diffusion coefficient in six types of random sphere packings, generated with different packing algorithms and parameters ($S \times 2$, $S \times 1$, $R \times 1$, $R \times 0.001$, $\Omega \times 0.05$, and $\Omega \times 0.95$). Fig. 6 presents the results for the simulated D_{eff} normalized by D_1 as a function of ϕ. At the first glance, the D_{eff}-ϕ data of the JT-packing types reflect their relative packing-scale disorder (Figs. 2(a) and 2(b)), with very similar values of the effective diffusive coefficient ($D_{\text{eff}}/D_1 \approx 0.67$) at $\phi = 0.634$ and maximal difference at $\phi = 0.54$, where the most homogeneous JT-packing type ($S \times 2$) has the highest value of $D_{\text{eff}}/D_1 = 0.73$ and the most heterogeneous JT-packing type ($R \times 0.001$) the lowest value of $D_{\text{eff}}/D_1 = 0.71$. R- and S-packings, however, have almost *identical* values of D_{eff} (within statistical variation) throughout the investigated packing density range. Because the common parameter in their generation is the value for the displacement length scaling-constant ($\alpha = 1$), the identical D_{eff}-ϕ curves for the R- and S-packings suggest that the influence of the packing microstructure on diffusion is restricted to the operative length scale of α, i.e., to the *local* environment of the individual spheres. Expressed in terms of the packing void space, the value of α affects the pores and the pathways to adjacent pores, the pore throats.

MC-packings are generally less tortuous than JT-packings, with D_{eff}/D_1 values between ~0.75 at $\phi = 0.54$ and $D_{\text{eff}}/D_1 = 0.70$ ($\Omega \times 0.05$) or $D_{\text{eff}}/D_1 = 0.69$ ($\Omega \times 0.95$) at $\phi = 0.634$. Differences between the two MC-packing types emerge and increase upon densification, as was observed for the DOH (Figs. 2(a) and 2(b)), but the $\Omega \times 0.05$ packing type

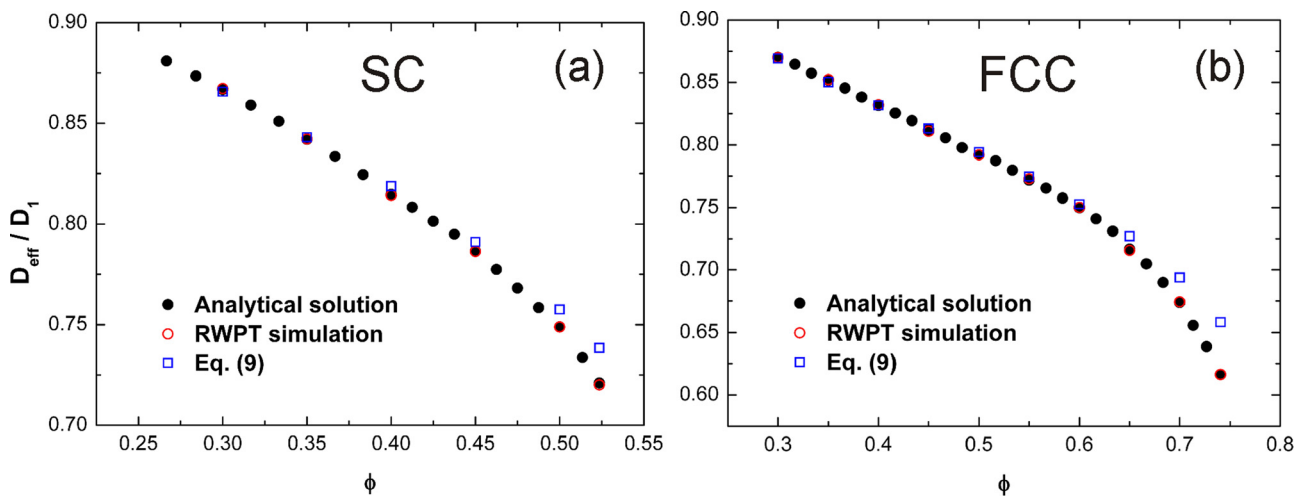

FIG. 5. Normalized effective diffusion coefficient D_{eff}/D_1 in SC (a) and FCC (b) sphere arrays, obtained from the analytical solution (Ref. 74; solid circles), with RWPT simulation (open circles), and by Eq. (9) (open squares).

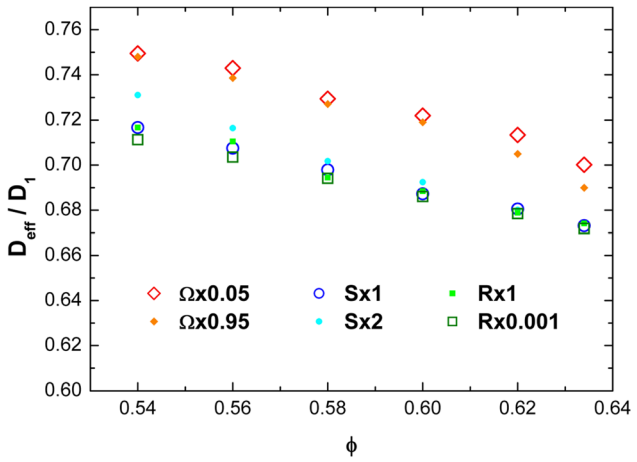

FIG. 6. Normalized effective diffusion coefficient D_{eff}/D_1 simulated with the RWPT approach in random sphere packings as a function of the solid volume fraction.

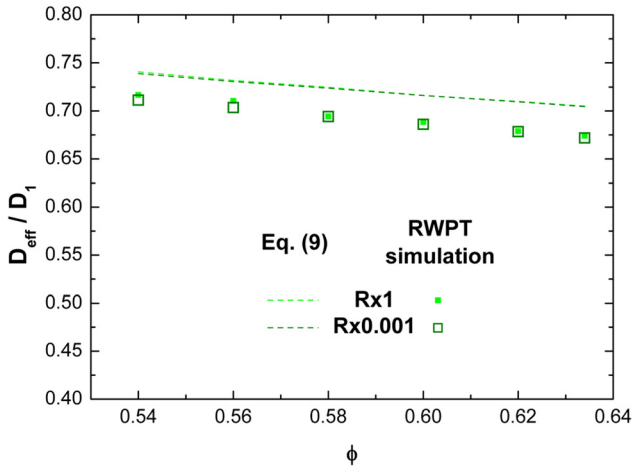

FIG. 8. Normalized effective diffusion coefficient D_{eff}/D_1 for the R-packings obtained with RWPT simulation (symbols) and calculated by Eq. (9) (dashed lines) as a function of the solid volume fraction.

maintains the *highest* D_{eff} among all packing types throughout the whole range of ϕ. This contrasts with the observation that at high ϕ (0.62 and 0.634) the $\Omega \times 0.05$ packing type has the largest DOH of all packing types (Figs. 2(a) and 2(b)), and is thus another indicator that the packing-scale disorder is not the determining factor for D_{eff}.

Figure 6 demonstrates that the microstructure of bulk, monodisperse, random sphere packings influences the effective diffusion coefficient. Although the effect is small -2% difference between the extreme JT-packing types $S \times 2$ and $R \times 0.001$ at $\phi = 0.54$, and similarly ca. 2% difference between the two MC-packing types at $\phi = 0.634$—it is genuine and not due to statistical variations among individual packings of a given type and sphere volume fraction, as the confidence intervals for D_{eff} do not exceed 1% of the D_{eff} values.

In Fig. 7, we compare the normalized D_{eff} simulated for the MC-packing types ($\Omega \times 0.05$ and $\Omega \times 0.95$) with values calculated according to Eq. (9). Both the simulated data and the data obtained with Eq. (9) demonstrate the same behavior regarding packing density: D_{eff} decreases with ϕ. However, $\Omega \times 0.05$ and $\Omega \times 0.95$ packings are characterized by different D_{eff} at a given ϕ. At the lowest solid volume fraction we analyzed ($\phi = 0.54$), the values of D_{eff} are almost identical, whereas D_{eff} values become distinct at higher ϕ. This distinction can be explained only by the difference in microstructures of $\Omega \times 0.05$ and $\Omega \times 0.95$ packings. During the RWPT simulations, the local diffusive displacements of the tracers directly reflect the specificity of the packing microstructure. For a given value of ϕ, the only parameter affecting the value of D_{eff} in Eq. (9) is ζ_2. Figure 7 indicates that this microstructural parameter is very sensitive to the packing morphology.

Figures 8 and 9 present a comparison of normalized effective diffusion coefficients simulated in the R- and S-packings with the values of D_{eff}/D_1 obtained by the approximation formula Eq. (9). Though, similar to the MC-packings, Eq. (9) overestimates the value of D_{eff} by a few percent enabling one to obtain a good estimate for the effective diffusion coefficient of an individual packing.

In Fig. 10, we summarize the data for all six packing types, obtained by the computer simulations and with the

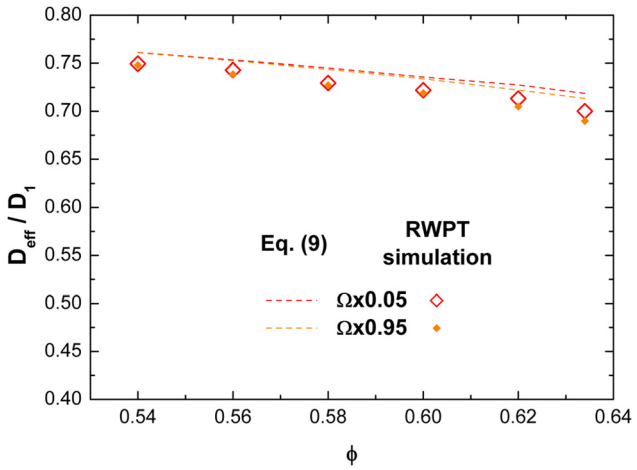

FIG. 7. Normalized effective diffusion coefficient D_{eff}/D_1 for the MC-packings obtained with RWPT simulation (symbols) and calculated by Eq. (9) (dashed lines) as a function of the solid volume fraction.

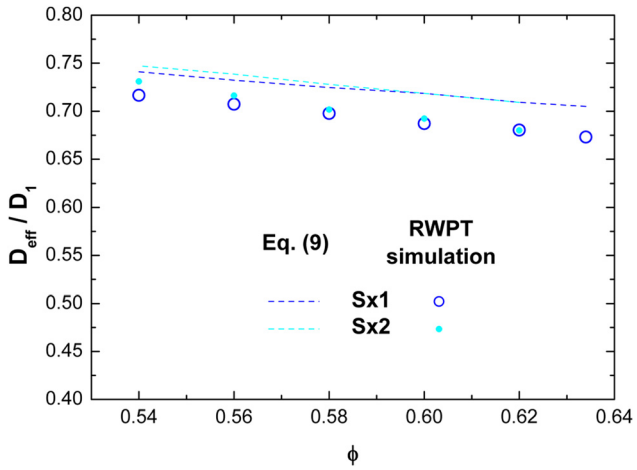

FIG. 9. Normalized effective diffusion coefficient D_{eff}/D_1 for the S-packings obtained with RWPT simulation (symbols) and calculated by Eq. (9) (dashed lines) as a function of the solid volume fraction.

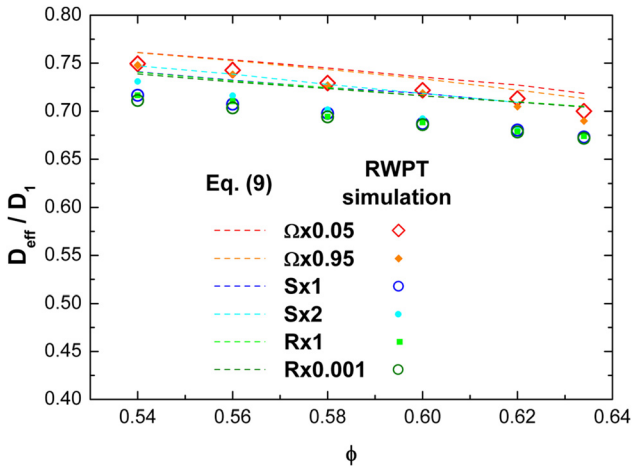

FIG. 10. Normalized effective diffusion coefficient D_{eff}/D_1 for all investigated random sphere packings obtained with RWPT simulation (symbols) and calculated by Eq. (9) (dashed lines) as a function of the solid volume fraction.

approximation formula Eq. (9). The results shown in Fig. 10 indicate that approximation (9) for the effective diffusion coefficient is able to distinguish microstructural differences in the various packing arrangements, as was originally shown by Torquato for the effective conductivity of packings of spheres.[13] Though Eq. (9) provides slightly overestimated values of D_{eff} in the random sphere packings (the relative error does not exceed 3.4%, 4.7%, and 4.9% for the MC-, S-, and R-packings, respectively), the use of this expression allows to determine effective diffusion coefficients with sufficiently high accuracy by accounting for packing geometry via the three-point parameter ζ_2 the packing geometry.

V. CONCLUSIONS

This work reports on numerical simulations of the effective diffusion coefficient in bulk random packings of monosized hard spheres. Six packing types were generated with different algorithms and parameters, resulting in a systematically varied degree of microstructural heterogeneity. We have verified that the corresponding predictions of Torquato's approximation formula (9), that the effective diffusion coefficient in random sphere packings is not fully defined by the solid volume fraction, but also depends on the packing type. These results demonstrate that a characterization of effective transport properties of sphere packings exclusively from the volume fraction can lead to an erroneous estimation of their effective transport parameters. The effective transport properties of sphere packings are also influenced by the morphology of a packing, which must be accounted for with an adequate description of the structure–transport relationships. For the first time, we have compared simulated effective diffusion coefficients for random sphere packings with corresponding predictions obtained from Torquato's approximation formula (9), which involves the three-point microstructural parameter ζ_2.[13] The comparison shows that this microstructure-sensitive parameter reflects the specificity of the morphology in individual sphere packings and, as a result, Eq. (9) provides accurate estimates of the effective diffusion coefficient for the wide class of random packings considered in this paper. The presented approach provides a straightforward route to quantitative structure–transport relationships for heterogeneous materials in general.

ACKNOWLEDGMENTS

We thank the John von Neumann Institute for Computing (NIC) and the Jülich Supercomputing Center (JSC), Forschungszentrum Jülich (FZJ, Jülich, Germany), for the allocation of special CPU-time grants (NIC Project Nos.: 5658 and 6550, JSC project ID: HMR10). S.T. was supported by the US Department of Energy, Office of Basic Energy Sciences, Division of Materials Sciences and Engineering, under Award No. DE-FG02-04-ER46108.

[1]S. Torquato, *Random Heterogeneous Materials: Microstructure and Macroscopic Properties* (Springer, New York, 2002).
[2]M. Sahimi, *Heterogeneous Materials: Vol. I. Linear Transport and Optical Properties* (Springer, New York, 2003).
[3]M. Sahimi, *Flow and Transport in Porous Media and Fractured Rock: From Classical Methods to Modern Approaches* (Wiley-VCH, Weinheim, Germany, 2011).
[4]T. I. Zohdi and P. Wriggers, *Introduction to Computational Micromechanics* (Springer, New York, 2005).
[5]S. Torquato, Appl. Mech. Rev. **44**, 37 (1991).
[6]W. F. Brown, Jr., J. Chem. Phys. **23**, 1514 (1955); Trans. Soc. Rheol. **9**, 357 (1965).
[7]S. Prager, Phys. Fluids **4**, 1477 (1961); Chem. Eng. Sci. **18**, 227 (1963); S. Prager, Physica **29**, 129 (1963).
[8]M. Beran and J. Molyneux, Q. Appl. Math. **24**, 107 (1966).
[9]M. Beran, Nuova Cimento **38**, 771 (1965).
[10]M. J. Beran and N. R. Silnutzer, J. Compos. Mater. **5**, 246 (1971).
[11]W. Strieder and R. Aris, *Variational Methods Applied to Problems of Diffusion and Reaction* (Springer, New York, 1973).
[12]G. W. Milton and K. Golden, in *Proceedings of the 18th International Thermal Conductivity Congress, Rapid City, USA, 3–5 October 1983*, edited by T. Ashworth and D. R. Smith (Plenum Press, New York, 1985), pp. 571–582.
[13]S. Torquato, J. Appl. Phys. **58**, 3790 (1985).
[14]A. K. Sen and S. Torquato, Phys. Rev. B **39**, 4504 (1989).
[15]L. Tartar, in *Nonlinear Analysis and Mechanics*, edited by R. J. Knops (Pittman Press, Boston, 1979), pp. 136–211.
[16]K. A. Lurie and A. V. Cherkaev, Proc. R. Soc. Edinburgh A **99**, 71 (1984); *ibid.* **104**, 21 (1986).
[17]G. A. Francfort and F. Murat, Arch. Ration. Mech. Anal. **94**, 307 (1986).
[18]R. V. Kohn and G. W. Milton, in *Homogenization and Effective Moduli of Materials and Media*, edited by J. L. Ericksen, D. Kinderlehrer, R. V. Kohn, and J. L. Lions (Springer, New York, 1986), pp. 97–125.
[19]G. W. Milton, Commun. Pure Appl. Math. **43**, 63 (1990).
[20]G. W. Milton, Commun. Math. Phys. **111**, 281 (1987).
[21]Z. Hashin and S. Shtrikman, J. Appl. Phys. **33**, 3125 (1962).
[22]S. Torquato, Ph.D. dissertation, State University of New York at Stony Brook, 1980.
[23]G. W. Milton, Phys. Rev. Lett. **46**, 542 (1981).
[24]S. Torquato, J. Chem. Phys. **84**, 6345 (1986).
[25]J. D. Beasley and S. Torquato, J. Appl. Phys. **60**, 3576 (1986).
[26]A. P. Cocco, G. J. Nelson, W. M. Harris, A. Nakajo, T. D. Myles, A. M. Kiss, J. J. Lombardo, and W. K. S. Chiu, Phys. Chem. Chem. Phys. **15**, 16377 (2013).
[27]G. Möbus and B. J. Inkson, Mater. Today **10**, 18 (2007).
[28]H. Koku, R. S. Maier, K. J. Czymmek, M. R. Schure, and A. M. Lenhoff, J. Chromatogr. A **1218**, 3466 (2011).
[29]T. Müllner, A. Zankel, C. Mayrhofer, H. Reingruber, A. Höltzel, Y. Lv, F. Svec, and U. Tallarek, Langmuir **28**, 16733 (2012).
[30]Z. Saghi and P. A. Midgley, Annu. Rev. Mater. Res. **42**, 59 (2012).
[31]G. Van Tendeloo, S. Bals, S. Van Aert, J. Verbeeck, and D. Van Dyck, Adv. Mater. **24**, 5655 (2012).
[32]T. Aste, M. Saadatfar, and T. J. Senden, Phys. Rev. E **71**, 061302 (2005).
[33]H. Dong and M. J. Blunt, Phys. Rev. E **80**, 036307 (2009).

[34]C. J. Gommes, A.-J. Bons, S. Blacher, J. H. Dunsmuir, and A. H. Tsou, AIChE J. **55**, 2000 (2009).
[35]F. Chevillotte, C. Perrot, and E. Guillon, J. Acoust. Soc. Am. **134**, 4681 (2013).
[36]J. T. Fredrich, B. Menendez, and T. F. Wong, Science **268**, 276 (1995).
[37]S. Bruns, T. Müllner, M. Kollmann, J. Schachtner, A. Höltzel, and U. Tallarek, Anal. Chem. **82**, 6569 (2010).
[38]S. Bruns and U. Tallarek, J. Chromatogr. A **1218**, 1849 (2011).
[39]S. Bruns, J. P. Grinias, L. E. Blue, J. W. Jorgenson, and U. Tallarek, Anal. Chem. **84**, 4496 (2012).
[40]K. Hormann and U. Tallarek, J. Chromatogr. A **1312**, 26 (2013).
[41]J. D. Seymour and P. T. Callaghan, AIChE J. **43**, 2096 (1997).
[42]U. Tallarek, E. Bayer, D. van Dusschoten, T. Scheenen, H. Van As, G. Guiochon, and U. D. Neue, AIChE J. **44**, 1962 (1998).
[43]B. Manz, L. F. Gladden, and P. B. Warren, AIChE J. **45**, 1845 (1999).
[44]A. J. Sederman, P. Alexander, and L. F. Gladden, Powder Technol. **117**, 255 (2001).
[45]S. Torquato, T. M. Truskett, and P. G. Debenedetti, Phys. Rev. Lett. **84**, 2064 (2000).
[46]Y. Jiao and S. Torquato, Phys. Biol. **9**, 036009 (2012).
[47]O. Wiener, Abh. Math. Phys. Kl. Königl. Sächs. Gesell. Wissen. **32**, 509 (1912).
[48]B. Jönsson, H. Wennerström, P. G. Nilsson, and P. Linse, Colloid Polym. Sci. **264**, 77 (1986).
[49]P. Venema, R. P. W. J. Struis, J. C. Leyte, and D. Bedeaux, J. Colloid Interface Sci. **141**, 360 (1991).
[50]W. S. Jodrey and E. M. Tory, Phys. Rev. A **32**, 2347 (1985).
[51]R. S. Maier, M. R. Schure, J. P. Gage, and J. D. Seymour, Water Resour. Res. **44**, W06S03, doi:10.1029/2006WR005577 (2008).
[52]S. Khirevich, A. Höltzel, and U. Tallarek, Commun. Comput. Phys. **13**, 801 (2013).
[53]R. J. Hill, D. L. Koch, and A. J. C. Ladd, J. Fluid Mech. **448**, 213 (2001).
[54]A. Bezrukov, M. Bargieł, and D. Stoyan, Part. Part. Syst. Charact. **19**, 111 (2002).
[55]A. Z. Zinchenko, J. Comput. Phys. **114**, 298 (1994).
[56]N. Metropolis, A. W. Rosenbluth, M. N. Rosenbluth, A. N. Teller, and E. Teller, J. Chem. Phys. **21**, 1087 (1953).
[57]M. P. Allen and D. J. Tildesley, *Computer Simulation of Liquids* (Oxford University Press, New York, 1991), Chap. 4.4.
[58]M. R. Schure and R. S. Maier, J. Chromatogr. A **1126**, 58 (2006).
[59]A. Okabe, B. Boots, K. Sugihara, and S. N. Chiu, *Spatial Tessellations: Concepts and Applications of Voronoi Diagrams* (John Wiley & Sons Ltd., Chichester, England, 2000).
[60]J. D. Bernal, Proc. R. Soc. London A **280**, 299 (1964).
[61]J. L. Finney, Proc. R. Soc. London A **319**, 479 (1970).
[62]R. Jullien, P. Jund, and D. Caprion, Phys. Rev. E **54**, 6035 (1996).
[63]R. Y. Yang, R. P. Zou, and A. B. Yu, Phys. Rev. E **65**, 041302 (2002).
[64]S. Khirevich, A. Daneyko, A. Höltzel, A. Seidel-Morgenstern, and U. Tallarek, J. Chromatogr. A **1217**, 4713 (2010).
[65]S. Khirevich, A. Höltzel, A. Seidel-Morgenstern, and U. Tallarek, J. Chromatogr. A **1262**, 77 (2012).
[66]L. Oger, A. Gervois, J. P. Troadec, and N. Rivier, Philos. Mag. B **74**, 177 (1996).
[67]J. C. Gil Montoro and J. L. F. Abascal, J. Phys. Chem. **97**, 4211 (1993).
[68]F. Delay, P. Ackerer, and C. Danquigny, Vadose Zone J. **4**, 360 (2005).
[69]P. Szymczak and A. J. C. Ladd, Phys. Rev. E **68**, 036704 (2003).
[70]H. Brenner, Philos. Trans. R. Soc., A **297**, 81 (1980).
[71]W. Gropp, E. Lusk, and A. Skjellum, *Using MPI: Portable Parallel Programming with the Message-Passing Interface*, 2nd ed. (MIT Press, Cambridge, MA, 1999).
[72]C. A. Miller and S. Torquato, J. Appl. Phys. **68**, 5486 (1990).
[73]R. C. McPhedran and G. W. Milton, Appl. Phys. A **26**, 207 (1981).
[74]M. H. Blees and J. C. Leyte, J. Colloid Interface Sci. **166**, 118 (1994).